Journal of Sound and Vibration (2002) **256**(4), 773–786
doi:10.1006/jsvi.2001.4225, available online at http://www.idealibrary.com on IDEAL®

LETTERS TO THE EDITOR

CRACK VERSUS COUPLING MISALIGNMENT IN A TRANSIENT ROTOR SYSTEM

S. Prabhakar, A. S. Sekhar and A. R. Mohanty

Department of Mechanical Engineering, Indian Institute of Technology, Kharagpur-721 302, *India*.
E-mail: *amohanty@mech.iitkgp.ernet.in*

(*Received* 17 *September* 2001, *and in final form* 18 *December* 2001)

1. INTRODUCTION

In industrial rotor systems, rotor unbalance and shaft-to-shaft misalignment are two common sources of vibrations in addition to the major concern of vibration due to shaft crack. Not much literature is available on coupling misalignment (shaft-to-shaft) in spite of its importance in industrial world. Recently, few attempts [1–4] have been made to simulate coupling misalignment in rotor systems. Another important rotor fault, which can lead to catastrophic failure, if undetected, is fatigue cracks in the shaft. Vibrational behavior of cracked structures, in particular cracked rotors has received considerable attention in the last three decades [5].

The concepts of a continuous on-line monitoring system with real time reporting offers the promise of improved knowledge of the condition of a machine and therefore fewer uncertainties in the operating decisions. Edwards *et al.* [6] have provided a broad review of the state of the art in fault diagnosis techniques, with particular regard to rotating machinery. In the context of fault detection, in spite of the importance of both the problems, sensitivity studies and condition-monitoring aspects of rotors with cracks and misalignment are rarely found in the literature. Coupling misalignment is very common in rotors and produces symptoms similar to those of cracks in shafts. It is thus essential to distinguish the vibration signals due to crack from that of coupling misalignment to avoid the rotor failure. Imam *et al.* [7] list a series of different signatures and Sekhar and Srinivasa Rao [8] have studied the $1X$ and $2X$ components of vibrations response to distinguish crack from coupling misalignment. However, the works [7, 8] have used the steady state response of rotor system with crack and misalignment.

Vibration monitoring during start-up or shut-down is as important as during steady state operation to detect cracks and coupling misalignment especially for machines such as aircraft engines which start and stop quite frequently and run at high speeds. The vibration signals during machine start-up or shut-down are non-stationary in nature. Wavelets provide a timescale information of a signal, enabling the extraction of features that vary in time and thus can be used for damage detection [9].

In the present work, using finite element method (FEM), transient analysis with crack and coupling misalignment has been done separately for the same rotor to distinguish crack from coupling misalignment. Continuous wavelet transform (CWT) has been used to extract characteristic features from vibration response of these two flaws [10, 11] in rotor system.

0022-460X/02/$35.00

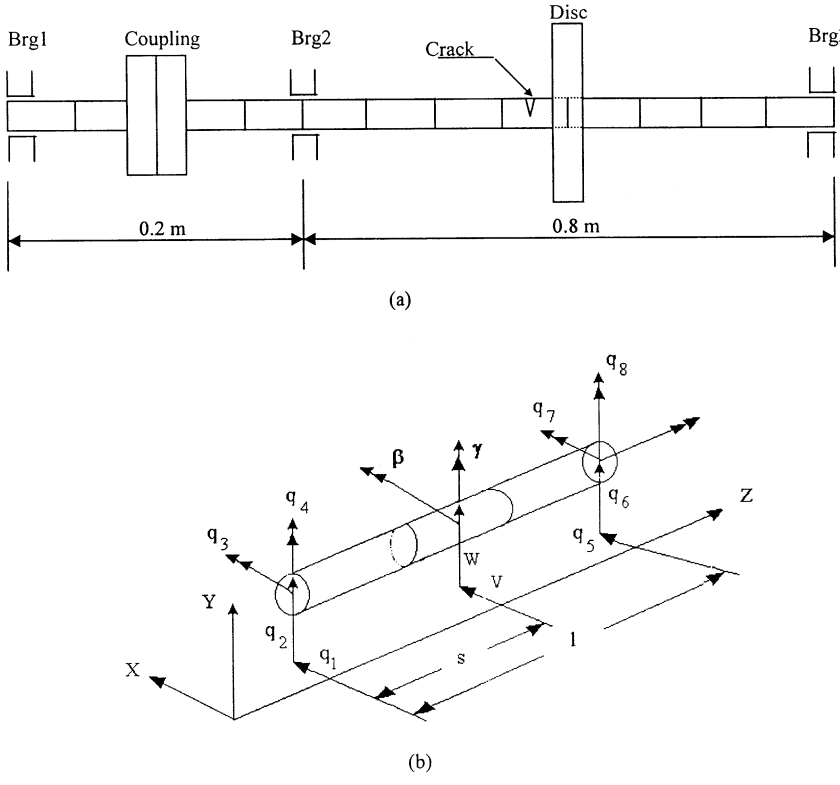

Figure 1. Rotor-coupling bearing system with typical finite rotor element details.

2. EQUATION OF MOTION

The rotor-coupling bearing system is discretized into finite beam elements as shown in Figure 1(a). A typical shaft rotor element is illustrated in Figure 1(b). Each element has two translational and two rotational degrees of freedom for bending mode at each node represented by q_1–q_8. The equation of motion of the complete rotor system in a fixed co-ordinate system can be written as

$$[M]\{\ddot{q}\} + [D]\{\dot{q}\} + [K]\{q\} = \{Q\}, \tag{1}$$

where the mass matrix $[M]$ includes the rotary and translational mass matrices of the shaft, mass and diametral moments of the rigid disc and the flexible coupling. The matrix $[D]$ includes the gyroscopic moments and the bearing damping. The stiffness matrix considers the stiffness of the shaft elements include cracked element, coupling element and the bearing stiffness. The details of the individual matrices of equation (1), except for the cracked element and coupling element, are given in references [12, 13]. The excitation matrix $\{Q\}$ in equation (1) consists of the unbalance forces and coupling misalignment forces. The details of crack and coupling modelling are given in the following section.

3. MODELLING OF CRACK AND FLEXIBLE COUPLING

3.1. TRANSVERSE CRACK

The transverse breathing crack has been considered for the present study. The flexibility matrices of the cracked section for flexural vibrations as given in Papadopoulos and

TABLE 1

Rotor-coupling-bearing data

Acceleration of the rotor, a	30 rad/s^2
Torque, Tq	30 N-m
Critical speed of the rotor-coupling bearing system (frictionless joint coupling)	1618 r.p.m. (26·98 Hz)
Shaft	
Diameter, D	20 mm
Density and modulus of elasticity	7800 kg/m^3, $2{\cdot}08 \times 10^{11}$ N/m^2
Disc	
Mass, m	5·5 kg
Polar moment of inertia, I_P	0·01546 kg-m^2
Diametral moment of inertia, I_D	0·00773 kg-m^2
Unbalance eccentricity, e	0·008 mm
Bearing (*isotropic*)	
Stiffness	$2{\cdot}5 \times 10^5$ N/m
Damping	100 N s/m
Coupling	
Type	Diaphragm coupling
Outer diameter	50 mm
Center of articulation, Z_3	75·15 mm
Bending spring rate per degree per disc pack, K_b	30 Nm/degree/disc pack
Parallel misalignment	
$\Delta X1$	0·1–0·7 mm
$\Delta Y1$	0·1–0·7 mm
Angular misalignment, θ_3	0·1°–0·5°

Dimarogonas [14] and utilized in FEM analysis of Sekhar and Prabhu [15] have been used for crack modelling. The flexibility coefficients for an element without crack by neglecting shearing action are given by

$$C_0 = \begin{bmatrix} l^3/3EI & & SYM & \\ 0 & l^3/3EI & & \\ 0 & -l^2/2EI & l/EI & \\ l^2/2EI & 0 & 0 & l/EI \end{bmatrix},$$

where EI is the bending stiffness and l is the element length.

The breathing action of the crack, i.e., its opening and closing as represented by Papadopoulos and Dimarogonas [16] is illustrated in Figure 2. During the shaft's rotation, the crack opens and closes, depending on the rotor deflection. For the large class of machines, the static deflection is much greater than the rotor vibration. With this assumption the crack is closed when $\phi = 0$ and it is fully open when $\phi = \pi$.

The transverse surface crack on the shaft element introduces considerable local flexibility due to strain energy concentration in the vicinity of the crack tip under load. The additional strain energy due to the crack results in a local flexibility matrix C_c which will be C_{op} and

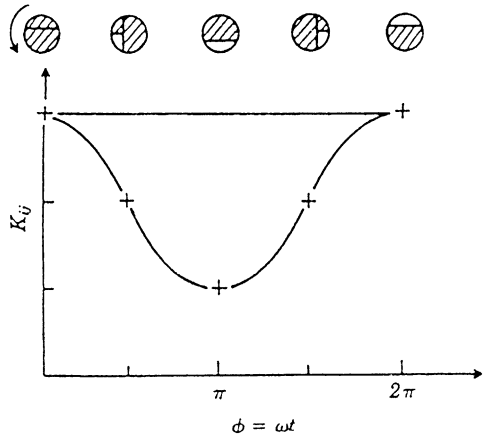

Figure 2. The breathing crack model.

C_{HC} for a fully open crack and half-open, half-closed conditions respectively:

$$C_{op} = \frac{1}{F_0}\begin{bmatrix} \bar{C}_{11}R & & SYM & \\ 0 & \bar{C}_{22}R & & \\ 0 & 0 & \bar{C}_{33}/R & \\ 0 & 0 & \bar{C}_{43}/R & \bar{C}_{44}/R \end{bmatrix},$$

$$C_{HC} = \frac{1}{2F_0}\begin{bmatrix} \bar{C}_{22}R & & SYM & \\ 0 & \bar{C}_{11}R & & \\ 0 & 0 & \bar{C}_{44}/R\mathrm{I} & \\ 0 & 0 & \bar{C}_{34}/R & \bar{C}_{33}/R \end{bmatrix},$$

where $F_0 = \pi ER^2/(1-\nu^2)$, $R = D/2$ and $\nu = 0{\cdot}3$. The dimensionless compliance coefficients, $\bar{C}_{ij}$, are computed from the derivations discussed in references [14, 16]. The total flexibility matrix for the cracked section is given as $[C] = [C_0] + [C_c]$.

From the equilibrium condition

$$(q_1, q_2, \ldots, q_8)^{\mathrm{T}} = [T]\,(q_5, \ldots, q_8)^{\mathrm{T}}, \tag{2}$$

where the transformation is

$$[T] = \begin{bmatrix} -1 & 0 & 0 & 0 \\ 0 & -1 & 0 & 0 \\ 0 & l & -1 & 0 \\ -l & 0 & 0 & -1 \\ 1 & 0 & 0 & 0 \\ 0 & 1 & 0 & 0 \\ 0 & 0 & 1 & 0 \\ 0 & 0 & 0 & 1 \end{bmatrix}.$$

The stiffness matrix of the cracked element is written as

$$[K_c] = [T][C]^{-1}[T]^{\mathrm{T}}. \tag{3}$$

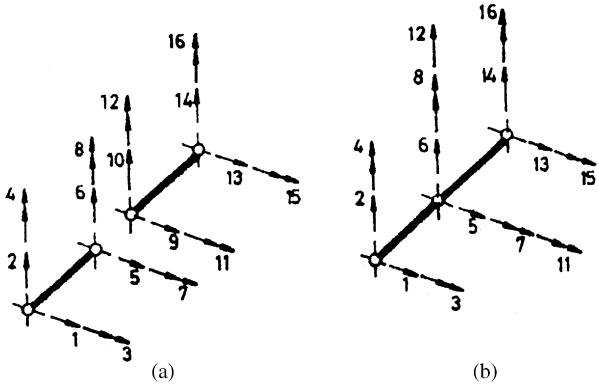

Figure 3. Co-ordinates of the two joined elements.

When the crack is assumed to affect only the stiffness, the stiffness matrix of the cracked element, $[K_c]$, replaces the stiffness matrix of the element which was originally uncracked, when assembling the stiffness matrix of the shaft, for $[K]$ in equation (1).

When the shaft is cracked, during the rotation the stiffness varies with time or with angle. The variation may be expressed by a truncated cosine series [16],

$$[K] = [K(\omega t)] = [K_0] + [K_1]\cos\omega t + [K_2]\cos 2\omega t + [K_3]\cos 3\omega t + [K_4]\cos 4\omega t, \tag{4}$$

where $[K_\eta]$, $\eta = 0, 1, \ldots, 4$, are fitting coefficient matrices, determined from the known behavior of the stiffness matrix at certain angular locations as explained by Papadopoulos and Dimarogonas [16]. Specifically,

$$[K] = [K]_{\phi=0} \text{ and } (\partial^2/\partial\phi^2)[K] = 0 \text{ at } \phi = \omega t = 0, \quad [K] = [K]_{\phi=\pi/2} \text{ at } \phi = \pi/2,$$
$$[K] = [K]_{\phi=\pi} \text{ and } (\partial^2/\partial\phi^2)[K] = 0 \text{ at } \phi = \omega t = \pi. \tag{5}$$

$[K]_{\phi=0}$, $[K]_{\phi=\pi/2}$ and $[K]_{\phi=\pi}$ are the stiffness matrices, K_{UC}, K_{op} and K_{HC} for the uncracked, fully open crack, and half-open, half-closed cracked conditions respectively. These are obtained from the compliance matrices C_o, C_{op} and C_{HC} respectively.

Application of conditions (5) to equation (4) yields the matrices $[K_\eta]$, $\eta = 0, 1, 2, 3, 4$, element by element as solution of 5×5 linear system of algebraic equations. The constant matrices of equation (4) are

$$[K_0] = (5K_{op} + 5K_{UC} + 6K_{HC})/16, \quad [K_1] = 9(K_{UC} - K_{op})/16,$$
$$[K_2] = (K_{op} + K_{UC} - 2K_{HC})/4, \quad [K_3] = (K_{op} - K_{UC})/16,$$
$$[K_4] = (-K_{op} - K_{UC} + 2K_{HC})/16. \tag{6}$$

3.2. FLEXIBLE COUPLING

Modelling of the flexible coupling as discussed by Kramer [17] is utilized in the present study. Two technical possibilities will arise while modelling the flexible couplings namely (i) a frictionless joint of (ii) a joint with stiffness and damping. In the present work the first possibility is considered.

For a frictionless radially stiff joint, the displacement at the two sides of the joint are identical and the angles are different. Figure 3(a) shows the co-ordinates of the two shaft

elements, which are to be joined. With $q_9 = q_5$ and $q_{10} = q_6$, the new co-ordinates are shown in Figure 3(b) for the elements when joined together. Then the stiffness matrix for this joint (coupling element) can be written as

$$[K_f] = \frac{EI}{l^3}\begin{bmatrix}
12 & & & & & & & & & & & & \\
0 & 12 & & & & & & & & & & & \\
0 & -6l & 4l^2 & & & & & & & & & & \\
6l & 0 & 0 & 4l^2 & & & & & & & & & \\
-12 & 0 & 0 & -6l & 24 & & & & & & & & \\
0 & -12 & 6l & 0 & 0 & 24 & & & & & & & \\
0 & -6l & -2l^2 & 0 & 0 & -6l & -4l^2 & & & & & & \\
6l & 0 & 0 & 2l^2 & 6l & 0 & 0 & 4l^2 & & & & & \\
0 & 0 & 0 & 0 & 0 & 0 & 0 & 6l & 4l^2 & & & & \\
0 & 0 & 0 & 0 & 0 & 0 & 6l & 0 & 0 & 4l^2 & & & \\
0 & 0 & 0 & 0 & 0 & 0 & -12 & 0 & 0 & -6l & 12 & & \\
0 & 0 & 0 & 0 & 0 & 0 & 0 & -12 & 6l & 0 & 0 & 12 & \\
0 & 0 & 0 & 0 & 0 & 0 & 0 & -6l & 2l^2 & 0 & 0 & -6l & 4l^2 \\
0 & 0 & 0 & 0 & 0 & 0 & 0 & 6l & 0 & 0 & 2l^2 & 6l & 0\ 4l^2
\end{bmatrix}.$$

(SYMMETRIC)

4. COUPLING MISALIGNMENT

Shaft misalignment is a condition in which the shafts of the driving and the driven machines are not on the same centerline. There are three possible types of coupling misalignments. (i) Angular—where the centerlines of the two shafts meet at an angle. (ii) Offset (parallel)—where the shafts centerlines are parallel but displaced from one another and (iii) a combination of angular and offset misalignment. Misalignment of machinery shafts causes reaction forces and moments to be generated in the coupling, which in turn affect the machines and are often a major cause of vibration. The reaction forces and moments, which are developed due to angular and parallel misalignment, are given in references [2, 8], have been used in the present analysis. The details are presented here briefly as these are introduced in the present work. Figure 4 shows two machine shaft centerlines, $Z1$ and $Z2$, which are misaligned. The centerline of the coupling spacer is shown connecting the two shaft centerlines with intersection points being the coupling centers of articulation, not the shaft's ends. The values and the directions of displacements $\Delta X1$, $\Delta Y1$, $\Delta X2$ and $\Delta Y2$ in Figure 4 can be obtained from the graphical plot of reverse indicator readings.

Assuming $Z1$ is the axis of the driving machine, that (+) torque is applied as shown in Figure 4 and the rotation is in the same direction as the applied torque, the reaction forces and moments, which the coupling exerts on the machine's shafts, are as follows [2, 8].

Parallel misalignment:

$$MX1 = Tq\sin\theta_1 + K_b\phi_1, \quad MY1 = Tq\sin\phi_1 - K_b\theta_1, \quad MZ1 = Tq,$$

$$MX2 = Tq\sin\theta_2 - K_b\phi_2, \quad MY2 = Tq\sin\phi_2 + K_b\theta_2, \quad MZ2 = -Tq,$$

$$FX1 = (-MY1 - MY2)/Z3, \quad FY1 = (MX1 + MX2)/Z3, \quad FZ1 = K_a\Delta Z + K_a(\Delta Z)^3,$$

$$FX2 = -FX1,\ FY2 = -FY1,\ FZ2 = FZ1.$$

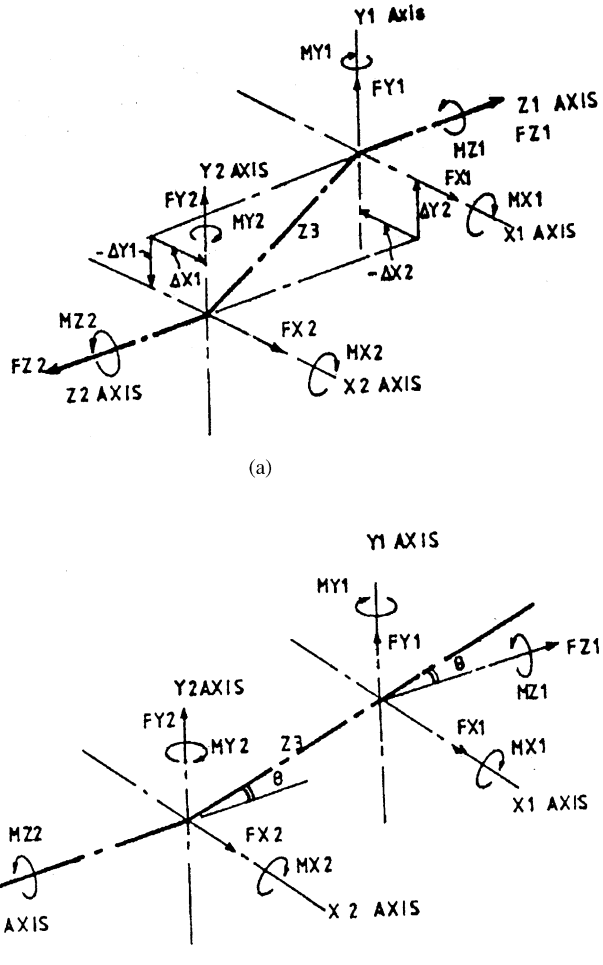

Figure 4. Coupling co-ordinate system. (a) parallel misalignment (b) angular misalignment.

Angular misalignment:

$$MX1 = 0{\cdot}0, \quad MY1 = 0{\cdot}0, \quad MZ1 = Tq/\cos\theta_3,$$

$$MX2 = -K_b\theta_3, \quad MY2 = Tq\sin\theta_3, \quad MZ2 = -Tq,$$

$$FX1 = (-MY1 - MY2)/Z3, \quad FY1 = (MX1 + MX2)/Z3, \quad FZ1 = K_a\Delta Z + K_a(\Delta Z)^3/\cos\theta_3,$$

$$FX2 = -FX1, \quad FY2 = -FY1, \quad FZ2 = FZ1.$$

In the present analysis, linear spring rates for the flexural couplings in both bending and axial nodes as assumed. Hence the term $(\Delta Z)^3$ is neglected in the above expressions, for this analysis.

The misalignment moments and the reaction forces are the static loads to the non-rotating observer. But they are acting as periodic loads on the rotating shafts with a periodic function of half-sinusoidal having a time period of π/ω. In the present work $1\,\omega$, $2\,\omega$, $3\,\omega$ and $4\,\omega$ components of the reaction forces are considered for coupling misalignment because stiffness variation of the crack is considered as a function of multiples

of operating speed up to 4ω (see equation (4)). The reaction force due to coupling misalignment are then incorporated into the excitation matrix $\{Q\}$ in the equation of motion (1) at the corresponding degrees of freedom. The nodal force vectors at the corresponding nodes due to coupling misalignment are given as

$$\{Q_c^1\} = \begin{Bmatrix} FX1\sin\omega t + FX1\sin 2\omega t + FX1\sin 3\omega t + FX1\sin 4\omega t \\ FY1\cos\omega t + FY1\cos 2\omega t + FY1\cos 3\omega t + FY1\cos 4\omega t \\ 0 \\ 0 \end{Bmatrix}, \tag{7}$$

$$\{Q_c^2\} = \begin{Bmatrix} FX2\sin\omega t + FX2\sin 2\omega t + FX2\sin 3\omega t + FX2\sin 4\omega t \\ FY2\cos\omega t + FY2\cos 2\omega t + FY2\cos 3\omega t + FY2\cos 4\omega t \\ 0 \\ 0 \end{Bmatrix}, \tag{8}$$

where $[Q_c^1]$ and $\{Q_c^2\}$ are the nodal force vectors at the left and right side of the coupling.

5. RESULTS AND DISCUSSION

A typical rotor-coupling bearing system as shown in Figure 1 has been considered in the present analysis. The rotor-coupling-bearing data used in the present study are given in Table 1. The analysis has been carried out by considering a crack and an angular misalignment of the coupling in the rotor system separately, using FEM for flexural vibrations. The rotor system is discretized into ten finite elements. In this work, the non-dimensional crack depth ($\bar{\alpha}$) is defined as the ratio of crack depth (α) to the shaft diameter (D). When the speed of rotation is changing, the angular rotation can be taken as $\theta(t) = \omega_0 t + 1/2\,(at^2)$, where a is the angular acceleration of rotor, ω_0 is the initial angular velocity and t is the time. The Houbolt time marching technique is used to model the system in time domain with a time step of 0·001 s. The Morlet mother wavelet with a support length of $(-4, 4)$ was chosen in the present study for all the continuous wavelet transforms [18]. The center frequency and bandwidth of the mother wavelet can be calculated, which in turn can be used for calculating the center frequency of daughter wavelets.

The scale of the CWT is chosen such that the centre frequency of the daughter wavelet in the frequency domain should not coincide with the critical and sub-critical speeds. If center frequency of daughter wavelet coincides with critical speeds, the CWT coefficients at those speeds will be high and will not show the details at the other significant speeds. The scale 35 has been chosen for all the CWTs since the center frequency of daughter wavelet (14·3 Hz) will not coincide with the critical (27 Hz) and sub-critical speeds.

Figure 5 shows the time responses for different crack depths and the corresponding CWT coefficient plots of the rotor passing the critical speed with an acceleration of 30 rad/s^2. In all the cases, time response has been modelled at bearing number two of the rotor system (see Figure 1). The rise of vibration amplitudes with crack depth can be seen from both the plots. However, the sub-critical response peaks are clearly evident from the CWT plots and these peaks are more apparent as the crack depth increases. This feature cannot be seen from the time history plots.

Similarly, Figure 6 shows the time response and the corresponding CWT plots for a typical rotor-coupling bearing system with and without angular misalignments for the same rotor with an acceleration of 30 rad/s^2. However, here no crack is present. A clear

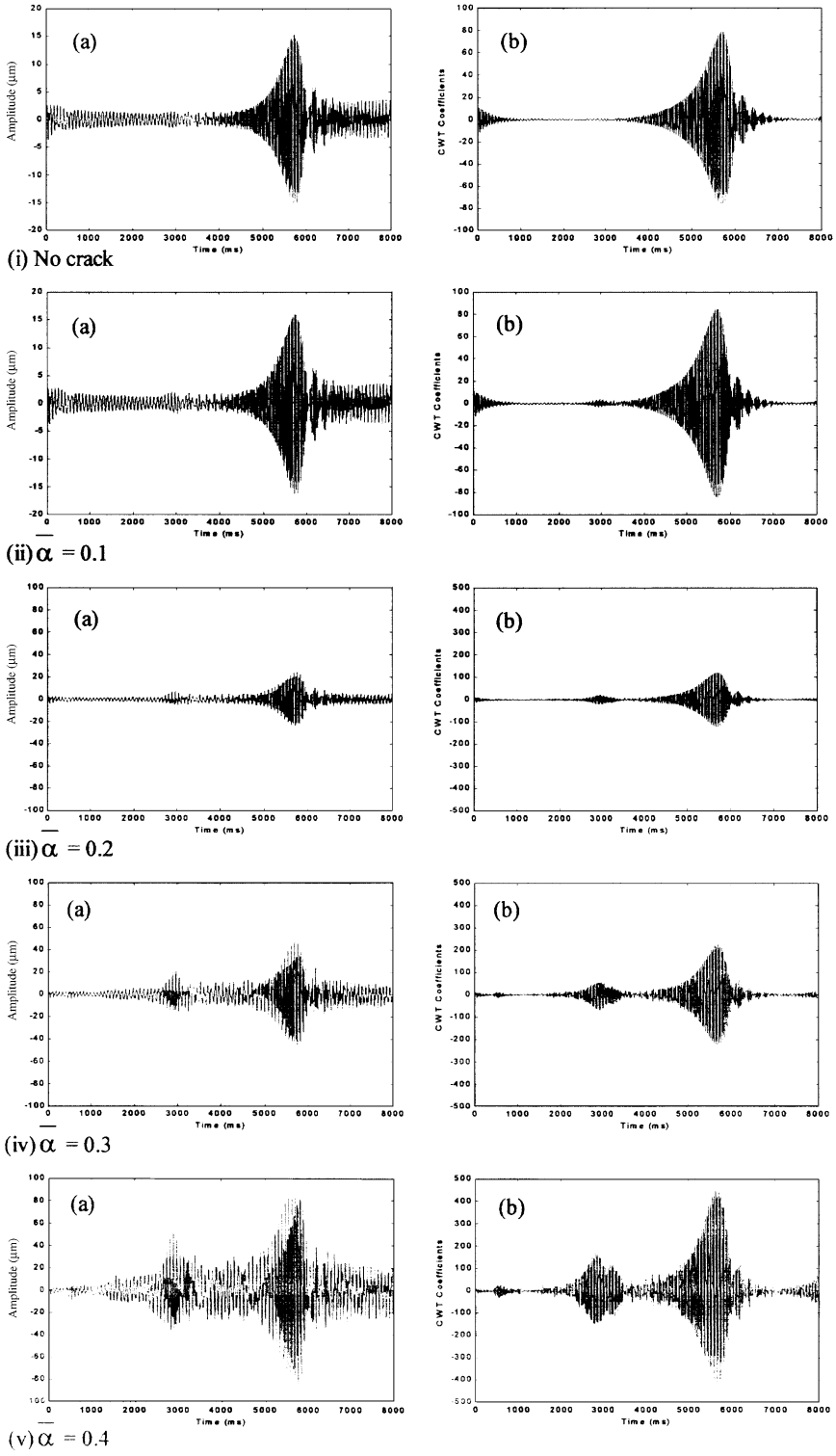

Figure 5. Time response and CWT coefficient plots of a rotor system for different crack depths; $a = 30$ rad/s^2. (a) Time (b) CWT.

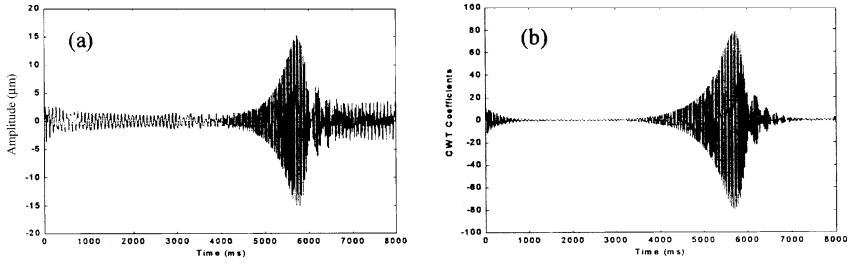

(i) without misalignment

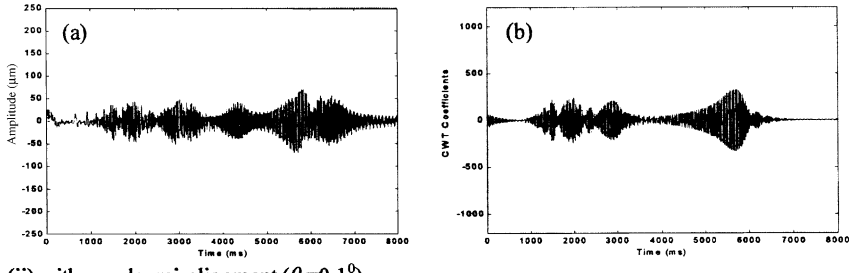

(ii) with angular misalignment ($\theta = 0.1^{0}$)

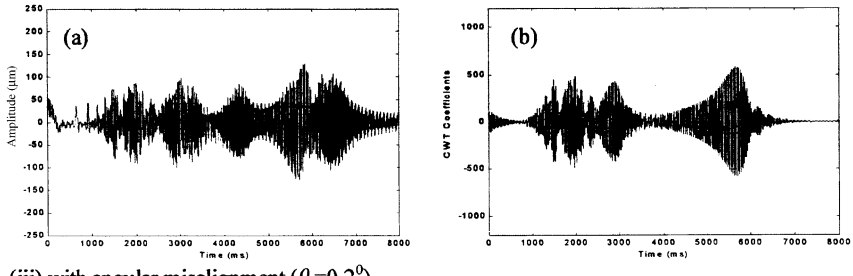

(iii) with angular misalignment ($\theta = 0.2^{0}$)

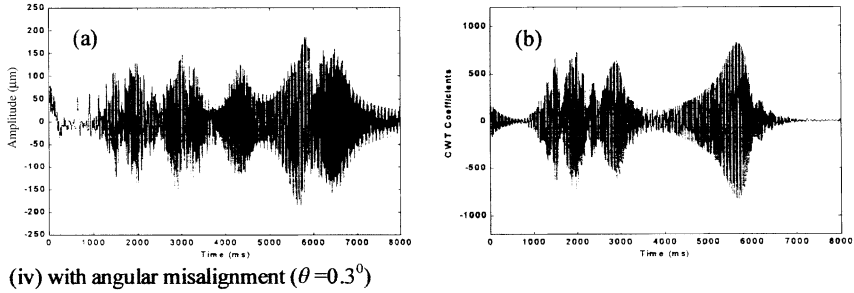

(iv) with angular misalignment ($\theta = 0.3^{0}$)

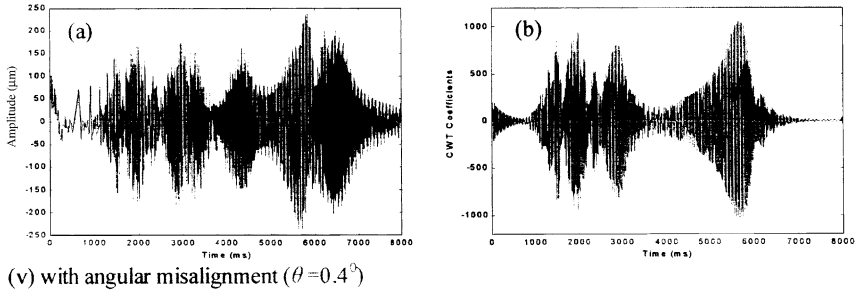

(v) with angular misalignment ($\theta = 0.4^{0}$)

Figure 6. Time response and CWT coefficients plot of a rotor system with a coupling having frictionless joint; $a = 30$ rad/s^2. (a) Time (b) CWT.

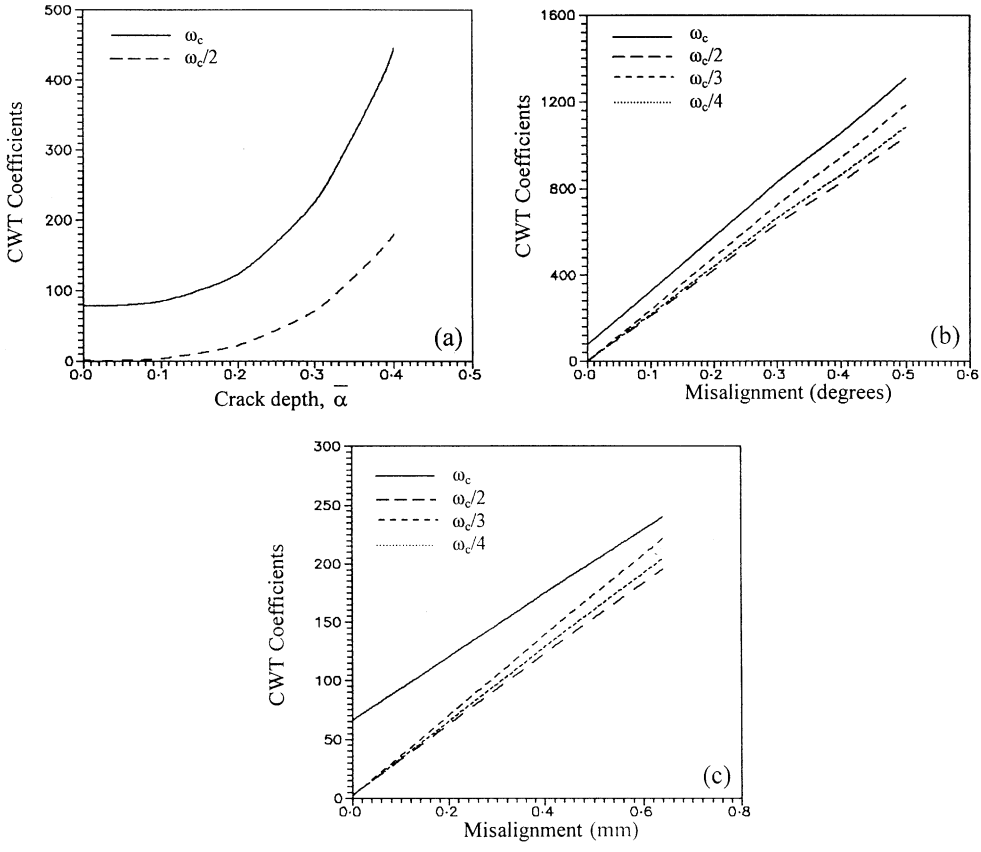

Figure 7. Variation of wavelet coefficients at critical and sub-critical speeds of a rotor system with crack and misalignment; $a = 30\,\text{rad/s}^2$. (a) crack (b) angular misalignment (c) parallel misalignment.

change in the pattern of time response is observed, but no clear features of misalignment are noted in the time response. In the case of CWT coefficient plots, the sub-harmonic resonant peaks at one-half, one-third and one-fourth the critical speed are evident when the misalignment is present in the system. These sub-critical speeds are not observed in time response as well as in CWT plot when the rotor-coupling bearing system is free from misalignment. Same features are also observed when parallel misalignment is present in the rotor system (results are not presented here). In both Figures 5 and 6, it can be observed that the presence of sub-harmonics in the CWT coefficient plot is the symptom of crack as well as coupling misalignment in a rotor system. However, the sub-harmonic resonant peaks at one-third and one-fourth the critical speed are not evident in the case of cracked rotor unlike in the case of misaligned rotor system.

Even though the symptom of the presence of sub-harmonic peaks is common in both these types of rotor flaws, it can be shown that there exists some difference in their behavior. The variations of CWT coefficients at critical and sub-critical speeds with crack depth as well as misalignment in their respective cases are shown in Figure 7. It is clear from Figure 7(a) that the variation of CWT coefficients with crack depth at critical and sub-critical speeds of cracked rotor is parabolic. But, in the case of misaligned rotor system, the variation of CWT coefficients is linear with the amount of misalignment in both cases of angular and parallel misalignments (see Figure 7(b, c)).

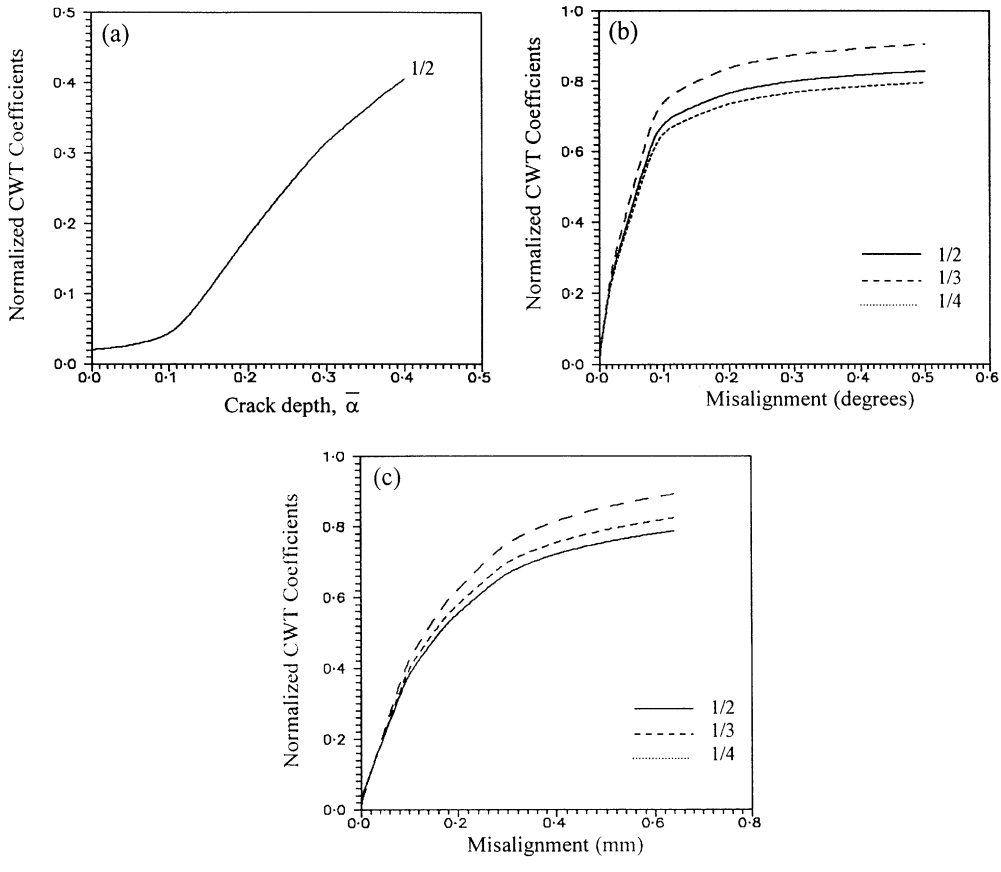

Figure 8. Variation of strength of sub-harmonics of a rotor system with crack and misalignment; $a = 30\,\text{rad/s}^2$. (a) crack (b) angular misalignment (c) parallel misalignment.

Further, the strength of sub-harmonics is different in both the cases of rotor flaws. The strength of sub-harmonics in Figure 8 is defined as the ratio of CWT coefficient at sub-critical speed to that of critical speed of the rotor system. The strength of sub-harmonic peak is weak of the order of 0·4 times the critical speed for maximum crack depth ($\bar{\alpha} = 0{\cdot}4$). But in the case of misaligned rotor system, the strength of sub-harmonic peaks is strong, of the order of 0·7–0·9 times the critical speed for high misalignments in both cases.

Also, it can be noticed from Figure 8(a–c) that the rate of change of sub-harmonic peak strength with crack depth is low for lower crack depths ($\bar{\alpha} < 0{\cdot}1$) and high for higher crack depths ($\bar{\alpha} > 0{\cdot}1$). In the case of misaligned rotor, the rate of change of sub-harmonic peak strength is high for low misalignments ($< 0{\cdot}2^\circ$ and 0·2 mm) and low for high misalignments and remains almost constant. This behavior is completely opposite to that of the cracked rotor.

Another important observation from Figure 8 can be made regarding detection and monitoring. CWT is very sensitive to small misalignments as compared to small crack depths. Thus, this is useful for the detection of coupling misalignment. However, from the monitoring point of view CWT is more useful for crack rather than misalignment.

Thus, this study helps to distinguish a crack from the coupling misalignment in a rotor system while it is passing through its critical speed.

6. CONCLUSIONS

The transient response of a rotor system with a crack and coupling misalignment has been used separately to distinguish each other. The CWT has been used as a tool for extracting the sub-harmonic resonant peaks from the time response of the cracked rotor as well as misaligned rotor while it is passing through its critical speed.

The presence of sub-harmonic at one-half the critical speed in the CWT coefficient plot is the symptom of crack while the presence of the sub-harmonic resonant peaks at one-half, one third and one-fourth the critical speed is the symptom of misalignment.

The strength of sub-harmonic peak with respect to critical is very weak in the case of cracked rotor as compared to that of misaligned rotor system. The rate of change of sub-harmonic peak strength with crack depth is low for lower crack depths and high for higher crack depths. In the case of misaligned rotor, the rate of change of sub-harmonic peak strength is high for low misalignments and low for high misalignments, and remains constant. CWT is useful for detection of coupling misalignment. But, from the monitoring point of view CWT is more useful for crack rather than misalignment in the rotor system. Thus, this study can be useful for distinguishing a crack from coupling misalignment in the rotor system.

REFERENCES

1. M. Xu and R. D. Marangoni 1994 *Journal of Sound and Vibration* **176**, 663–679. Vibration analysis of a motor-flexible coupling-rotor system subjected to misalignment and unbalance, Part—I: theoretical model and analysis.
2. A. S. Sekhar and B. S. Prabhu 1995 *Journal of Sound and Vibration* **185**, 655–671. Effects of coupling misalignment on vibrations of rotating machinery.
3. A. S. Sekhar and A. Srinivasa Rao 1996 41 *American Society of Mechanical Engineers International Gas Turbines & Aeroengine congress and Exhibition, Birmingham, UK*, Paper No. **96**-GT-12. Vibration analysis of rotor-coupling bearing system with misaligned shafts.
4. Y. S. Lee and C. W. Lee 1999 *Journal of Sound and Vibration* **224**, 17–32. Modelling and vibration analysis of misaligned rotor-ball bearing systems.
5. A. D. Dimarogonas 1996 *Engineering and Fracture mechanics* **55**, 831–857. Vibration of cracked structures: A state of the Art review.
6. S. Edwards, A. W. Lees, and M. I. Friswell 1998 *Shock and Vibration Digest* **30**. Fault diagnosis of rotating machinery.
7. I. Imam, S. H. Azzaro, R. J. Bankert and J. Scheibel 1989 *American Society of Mechanical Engineers Journal of Vibration, Acoustics, Stress and Reliability in Design* **111**, 241–250. Development of on-line rotor crack detection and monitoring system.
8. A. S. Sekhar and A. Srinivasa Rao 1996 *Journal of Machine Vibration* **5,** 179–188. Crack versus misalignment in rotor-coupling bearing system.
9. W. J. Staszewski 1998 *The Shock and Vibration Digest* **30**, 457–472. Structural and mechanical damage detection using wavelets.
10. S. Prabhakar, A. S. Sekhar and A. R. Mohanty 2001 *Journal of Mechanical Systems and Signal Processing* **15**(2), 447–450. Detection and monitoring of cracks in a rotor-bearing system using wavelet transforms.
11. S. Prabhakar, A. S. Sekhar and A. R. Mohanty 2001 *Journal of Mechanical Engineering Sciences, I Mech, Part-C*, **215**, 1417–1428. Vibration analysis of a misaligned rotor-coupling-bearing system passing through the critical speed.
12. H. D. Nelson and J. M. McVaugh 1976 *American Society of Mechanical Engineers Journal of Engineering for Industry* **98**, 593–600. The dynamics of rotor-bearing systems using finite elements.
13. H. N. Ozguven and Z. L. Ozkan 1984 *American Society of Mechanical Engineers Journal of Vibration, Acoustics Stress and Reliability in Design* **106**, 72–79. Whirl speeds and unbalance response of multi bearing rotor using finite elements.
14. C. A. Papadopoulos and A. D. Dimarogonas 1987 *Journal of Sound and Vibration* **117**, 81–93. Coupled longitudinal and bending vibrations with an open crack.

15. A. S. SEKHAR and B. S. PRABHU 1994 *Journal of Sound and Vibration* **173**, 415–421. Transient analysis of a cracked rotor passing through the critical speed.
16. C. A. PAPADOPOULOS and A. D. DIMAROGONAS 1988 *American Society of Mechanical Engineers Journal of Vibration, Acoustics, Stress and Reliability in Design* **110**, 356–359. Stability of cracked rotors in the coupled vibration mode.
17. E. KRAMER *Dynamics of Rotors and Foundations.* Berlin: Springer-Verlag, 224–226.
18. I. DAUBECHIES 1992 *Ten Lectures on Wavelets.* Philadelphia: SIAM.